DOI 10.1007/s11106-022-00265-1
Powder Metallurgy and Metal Ceramics, Vol. 60, Nos. 9-10, January, 2022 (Russian Original Vol. 60, Nos. 9-10, Sept.-Oct., 2021)

THEORY, PRODUCTION TECHNOLOGY, AND PROPERTIES OF POWDERS AND FIBERS

CHANGES IN THE PROPERTIES OF ULTRAFINE Al_2O_3–ZrO_2–Y_2O_3–CeO_2 POWDERS AFTER HEAT TREATMENT IN THE RANGE 400–1450°C

M.Yu. Smyrnova-Zamkova,[1,2] O.V. Dudnik,[1] O.I. Bykov,[1] O.K. Ruban,[1] and O.I. Khomenko[1]

UDC 541.182:621.762

Ultrafine 90AZK, 80AZK, 70AZK, and 58.5AZK powders in the Al_2O_3–ZrO_2–Y_2O_3–CeO_2 system were produced for the first time by a combined method involving hydrothermal synthesis followed by mechanical mixing with α-Al_2O_3 (HTSM). The properties of the powders heat treated in the range 400–1450°C were examined by differential thermal analysis, X-ray diffraction, electron microscopy, and nitrogen thermal adsorption–desorption (BET). The sizes of primary particles were calculated with the Scherrer equation. The AMIC (Automatic Microstructure Analyzer) software was applied to process the powder morphology analysis results. The F-ZrO_2 → T-ZrO_2 phase transformation was found to proceed completely when the powders were mechanically mixed in the HTSM process. The M-ZrO_2 phase was identified as traces in the ultrafine 90AZK and 80AZK powders after mechanical mixing, was not found in the 70AZK powder, and emerged as traces in the 58.5AZK powder above 1150℃. Heat treatment was shown to induce a topochemical memory effect in the ceramics: the morphology and shape factor of the ultrafine powders following heat treatment at 400–1450℃ varied topologically continuously. The dependence of primary particle sizes and specific surface area of the powders on the heat treatment temperature indicated that they had high sintering activity. The powders are needed to produce highly efficient ZTA composites in the Al_2O_3–ZrO_2–Y_2O_3–CeO_2 system, consisting of fine particles of the viscous zirconia-based solid solution, codoped with ceria and yttria, distributed in a rigid alumina matrix.

Keywords: *Al_2O_3–ZrO_2–Y_2O_3–CeO_2 system, ZTA composites, hydrothermal synthesis in an alkaline environment, mechanical mixing, shape factor, zirconia-based solid solution.*

[1]Frantsevich Institute for Problems of Materials Science, National Academy of Sciences of Ukraine, Kyiv, Ukraine.

[2]To whom correspondence should be addressed; e-mail: smirnovazamkova@ukr.net.

Translated from Poroshkova Metallurgiya, Vol. 60, Nos. 9–10 (541), pp. 3–16, 2021. Original article submitted August 10, 2021.

INTRODUCTION

The Al_2O_3–ZrO_2–Y_2O_3–CeO_2 system underlies the development of materials for different applications: tool, structural, medical, and functional. These materials feature high strength, heat resistance, wear resistance, and oxidation resistance, low thermal conductivity, and thermal expansion coefficients that are comparable to those possessed by metals. Zirconia-toughened alumina ceramics (ZTA ceramics) belong to precipitation-strengthened materials with an α-Al_2O_3 matrix that is toughened by pure zirconia particles or zirconia-based solid solutions. The properties of ZTA ceramics are determined by transformation hardening and microcracking mechanisms, governing the capability to control martensitic phase transformations of the toughening phase [1–3]. Targeted changes in the chemical and phase composition of the matrix and in the content and morphology of the particulate phases and variation in the methods to synthesize and pretreat the starting nanocrystalline and ultrafine powders are necessary conditions for the development of up-to-date oxide composites. The production of transformation-hardened ZTA materials is associated with thermodynamically nonequilibrium condition resulting from a significant number of phase transformations undergone by both alumina and zirconia.

The main attention is currently paid to ZTA composites with an α-Al_2O_3 matrix strengthened by yttria-stabilized T-ZrO_2 particles (Y-TZP). The ZTA composites that contain a zirconia-based solid solution stabilized by 3 mol.% Y_2O_3 have been studied in greatest detail [2, 4–7]. Current research efforts indicate that ceria favorably influences the mechanical properties and stability of T-ZrO_2 [8, 9]. The ZTA composites doped with ceria acquire improved properties when ceria is part of the zirconia-based solid solution [9, 10]. There are hardly any studies in the literature that would focus on ZTA composites with zirconia stabilized by both yttria and ceria. Study of ZTA composites having a substantial volume content of zirconia (>30 vol.%) or even equal volume contents of alumina and zirconia would also improve the understanding of the transformation hardening mechanism. The strength and hardness of such ZTA composites are believed to be improved through a synergetic action of superfine zirconia grains and stabilizing agents in the zirconia-based solid solution since metastable T-ZrO_2 that is capable of undergoing the T-ZrO_2 $\rightarrow$ M-ZrO_2 transformation under stresses is retained [11].

There is a direct relationship between the processes employed to produce the starting powders and the properties acquired by the resultant transformation-hardened ZTA materials. To impart the required properties to the materials, the starting powders should be produced in extremely nonequilibrium systems [12–14].

Hydrothermal synthesis in an alkaline environment belongs to wet chemical methods and combines the advantages of the sol–gel process, coprecipitation, and hydrothermal treatment and allows the particulate product morphology to be controlled through variation in the process parameters [15]. When nanosized particles in the Al_2O_3–ZrO_2–Y_2O_3–CeO_2 system that have been hydrothermally synthesized in an alkaline environment are heat treated, phase transformations of zirconia (metastable zirconia-based cubic solid solution $\rightarrow$ tetragonal zirconia-based solid solution (F-ZrO_2 $\rightarrow$ T-ZrO_2)) and boehmite (γ-AlO(OH) $\rightarrow$ Θ-Al_2O_3 $\rightarrow$ α-Al_2O_3) take place in parallel; i.e., several phases, zirconia and alumina, coexist on a permanent basis [16, 17].

To weaken the synergetic effect of alumina and zirconia phase transformations to produce powders of complex composition in the Al_2O_3–ZrO_2–Y_2O_3–CeO_2 system, a combined method involving hydrothermal synthesis of a nanocrystalline powder of the zirconia-based solid solution in an alkaline environment and its further mechanical mixing with an ultrafine α-Al_2O_3 powder (HTSM method) is advised [18]. Mechanical activation of the starting powders, at the earliest stages of creating a particulate system, is among the conditions needed for controlling the structure and properties of materials. The successive use of hydrothermal synthesis and mechanical mixing reduces uncertainties associated with the evolution of properties to be acquired by ultrafine powders of complex composition when they are produced and heat treated because there is no effect of the phase transformations of alumina on the phase transformations of the zirconia-based solid solution [18, 19] and mechanical mixing activates the nanocrystalline powders. The HTSM method is simple and safe, includes a minimum number of precursor preparation stages, and does not require complex chemical equipment or expensive reagents.

Our objective is to establish physicochemical properties of ultrafine powders in the Al_2O_3–ZrO_2–Y_2O_3–CeO_2 system containing 10 to 41.5 wt.% zirconia solid solution within the combined HTSM process and after heat treatment. The zirconia-based solid solution (ZrO_2 (Y_2O_3, CeO_2)) has constant composition, mol.%: 90 ZrO_2–2 Y_2O_3–8 CeO_2.

Well-grounded choice of the composition, insights into the basic laws behind phase transformations depending on temperature, and selection of an optimal sequence of processing steps are required for targeted microstructural design of advanced ZTA composites.

EXPERIMENTAL PROCEDURE

The main intention in choosing the test powder compositions was to strengthen the brittle alumina matrix with particles of a zirconia-based solid solution, characterized by high viscosity. The paper [20] shows that the $90ZrO_2$–$2Y_2O_3$–$8CeO_2$ composition (mol.%) is highly resistant to low-temperature degradation in humid environments and has K_{Ic} equal to 8 MPa · $m^{0.5}$. Hence, the zirconia solid solution of this composition was chosen for the experiment. The powders contained from 90 to 58.5 wt.% Al_2O_3. The ZTA powders chosen for the experiment are described in Table 1. The 58.5AZK powder composition corresponds to that of the binary eutectic in the Al_2O_3–ZrO_2 phase diagram [20, 21].

The starting reagents were zirconium oxychloride ($ZrOCl_2 \cdot 8H_2O$), yttrium nitrate ($Y(NO_3)_3 \cdot 6H_2O$), and cerium nitrate ($Ce(NO_3)_3 \cdot 6H_2O$); all reagents were of chemically pure grade. The alumina reagent was α-Al_2O_3 of Baikalox 23810-1 grade (produced by Universal Photonics Incorporated, USA) with a specific surface area of 5 m^2/g. The hydrothermal synthesis of a nanosized powder of the zirconia-based solid solution of composition (mol.%) 90 ZrO_2–2 Y_2O_3–8 CeO_2 in an alkaline environment is described in detail in [22]. The zirconia-based solid solution had a specific surface area of 94 m^2/g and contained the F-ZrO_2 phase.

TABLE 1. Compositions of Test Powders

Composition No.	Composition, wt.%	Notation
1	90 Al_2O_3–10 ZrO_2 (Y_2O_3, CeO_2)	90AZK
2	80 Al_2O_3–20 ZrO_2 (Y_2O_3, CeO_2)	80AZK
3	70 Al_2O_3–30 ZrO_2 (Y_2O_3, CeO_2)	70AZK
4	58.5 Al_2O_3–42.5 ZrO_2 (Y_2O_3, CeO_2)	58.5AZK

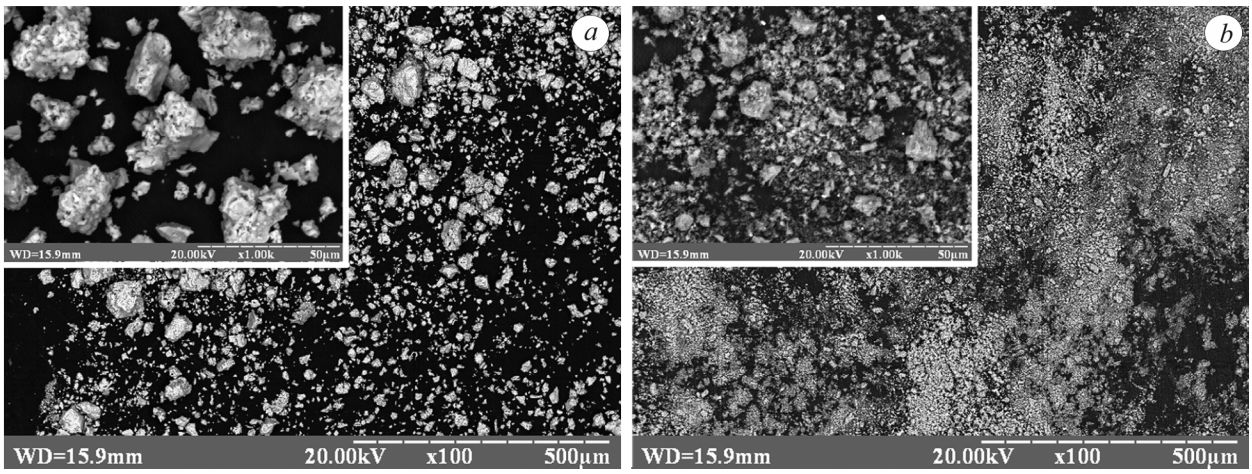

Fig. 1. SEM images of the nanocrystalline ZrO_2(CeO_2, Y_2O_3) powder (*a*) and ultrafine α-Al_2O_3 powder (*b*)

Morphologies of the starting powder of the ZrO_2 (CeO_2, Y_2O_3) solid solution and α-Al_2O_3 starting powder were examined by scanning electron microscopy (SEM). Figure 1 shows that the ZrO_2 (CeO_2, Y_2O_3) powder contains round and irregular agglomerates. The round agglomerates are actually in one size (~20 μm). The agglomerates are well seen (Fig. 1*a*) to consist of primary particle conglomerates. These conglomerates are within 5 μm in size. Individual irregular agglomerates reach 20 μm, but their main size fraction is 5–10 μm long. These agglomerates also contain primary particle conglomerates. The α-Al_2O_3 powder (Fig. 1*b*) contains within 5% of round agglomerates approximately 10–15 μm in diameter. The main size fraction includes agglomerates varying from 1 to 5 μm in size. These agglomerates are not solid either and consist of primary particle conglomerates.

To synthesize ultrafine 90AZK, 80AZK, 70AZK, and 58.5AZK powders, the ready-made α-Al_2O_3 powder and the nanosized ZrO_2(Y_2O_3, CeO_2) powder hydrothermally synthesized in an alkaline environment were mechanically mixed for 8 h in a planetary-ball mill in isopropyl alcohol. The mixtures were dried at 80°C for 24 h. To study how the physicochemical properties of the ultrafine powders evolved, they were heat treated at 400, 550, 700, 850, 1000, 1150, 1300, and 1450°C and held for 2 h at each temperature. The ultrafine powders were heat treated in a SNOL 7.2/1100 laboratory electrical furnace, muffle furnace, and Nabertherm LTH08/17 laboratory electrical furnace.

The properties of the powders after synthesis and heat treatment were examined by X-ray diffraction (XRD) (upgraded DRON-3M diffractometer, Cu-K_α radiation, Ni filter, and 1–4°/min scan rate at 2θ varying from 10 to 90°). The diffraction peaks were fitted to the Voigt and Gauss functions to refine their parameters. The Match software, PDF-2 X-Ray Powder Diffraction File, differential thermal analysis data (Q-1500D analyzer, 10°C/min heating rate in the range 20–1000°C), and electron microscopy (scanning electron microscope with a REM 106I energy-dispersive microanalyzer and ZEISS EVO 40XVPa scanning electron microscope) were used to identify phases.

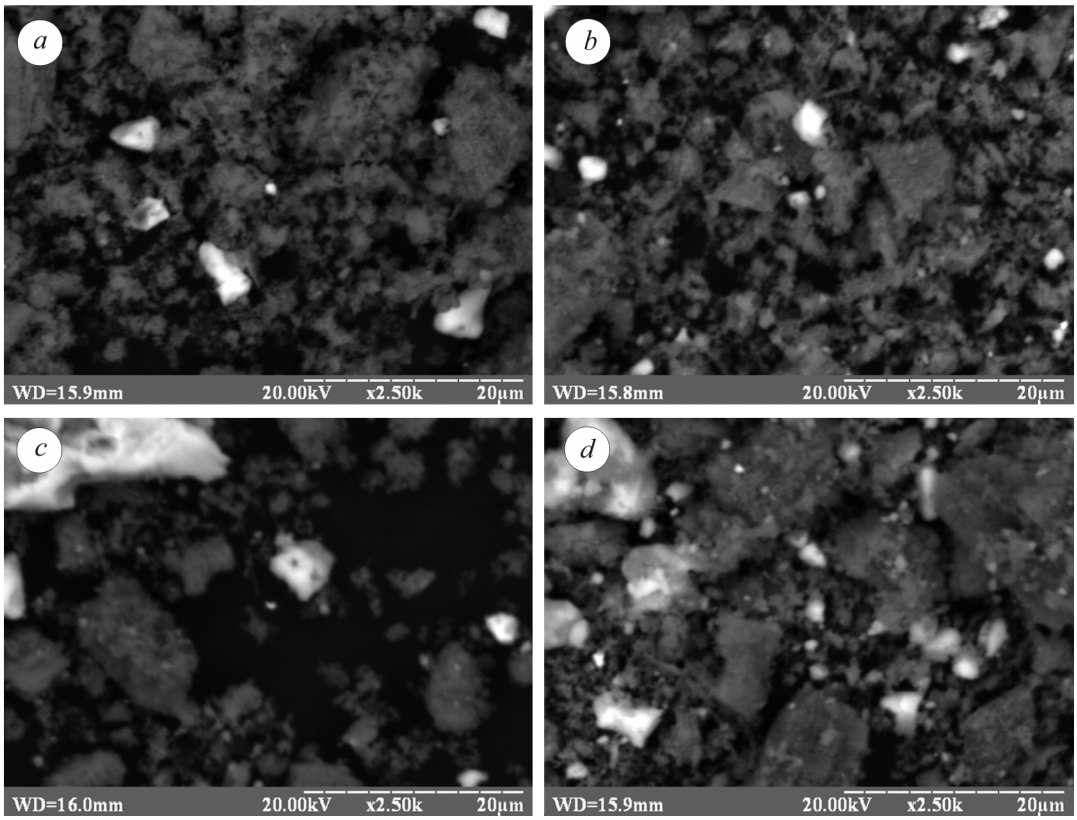

Fig. 2. SEM images of the ultrafine 90AZK (*a*), 80AZK (*b*), 70AZK (*c*), and 58.5AZK (*d*) powder agglomerates

The specific surface area of the powders was found by nitrogen thermal adsorption–desorption (BET method). The AMIC (Automatic Microstructure Analyzer) software [23] was used to process the powder morphology analysis data. The image processing algorithm intended to obtain quantitative metallography data is based on the Cavalieri–Aker–Glagolev principle [23, 24].

RESULTS AND DISCUSSION

According to XRD, T-ZrO_2 and traces of M-ZrO_2 were identified in the 90AZK and 80AZK starting mixtures besides α-Al_2O_3, and T-ZrO_2 was identified in the 70AZK and 58.5AZK mixtures. Hence, the F-ZrO_2 $\rightarrow$ T-ZrO_2 phase transformation occurred in the mechanical mixing process. The specific surface areas were 14 (90AZK), 24 (80AZK), 60 (70AZK), and 57 m^2/g (58.5AZK).

Figure 2 shows morphology of the ultrafine powders. Bimodal size distribution of the agglomerates is seen in the 90AZK and 80AZK powders. The 90AZK powder (Fig. 2*a*) contains ~10% of agglomerates within 10 μm in size, while their main size fraction is within 5 μm. The ratio of the two size fractions is almost 50 : 50 in the 80AZK powder (Fig. 2*b*). The agglomerates are dense in both cases. In the 70AZK powder (Fig. 2*c*), 5–10 μm agglomerates, being quite loose, are predominant. Figure 2*d* shows that the 58.5AZK powder has loose irregular agglomerates within 20 μm. These morphological features explain why the specific surface area of the mixtures

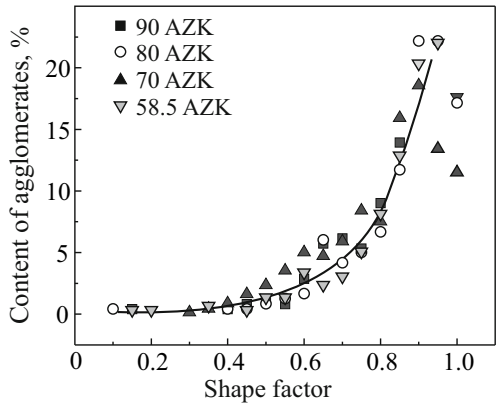

Fig. 3. Shape factor of the starting ultrafine powders in the Al_2O_3–ZrO_2–Y_2O_3–CeO_2 system

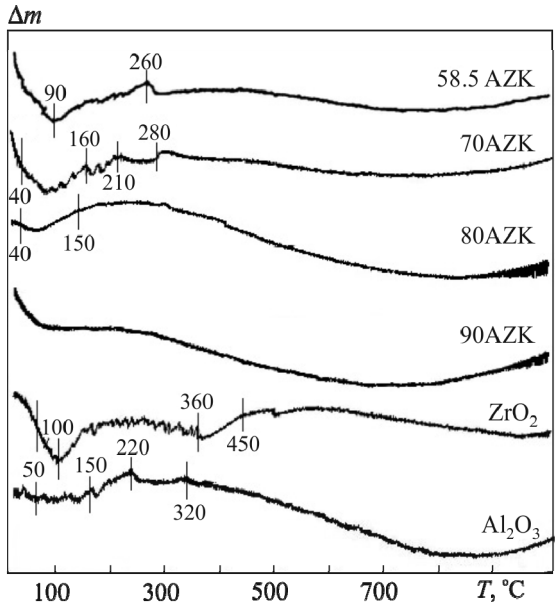

Fig. 4. DTA results for the synthesized ultrafine powders in the Al_2O_3–ZrO_2–Y_2O_3–CeO_2 system

changes: it increases when the agglomerates become more porous. Figure 3 demonstrates that agglomerates in the powders produced by the combined method are distributed in a similar way according to the shape factor.

Figure 4 shows DTA curves from the thermogravimetric patterns for the starting zirconia and alumina powders and resultant ZTA powders. These curves change with increasing content of the zirconia-based solid solution. The curves for the 90AZK and 80AZK powders are similar to that for the α-Al_2O_3 powder and the curves for the 70AZK and 58.5AZK powders are similar to that for the $ZrO_2(CeO_2, Y_2O_3)$ powder. The intensive endothermic effects on the DTA curves with minima at 90–100°C correspond to the removal of absorbed water and the endothermic effects at temperatures close to 300°C to the removal of crystallization and coordinately bound water. The exothermic effect, of much lower intensity, corresponds to the transition of the zirconia-based solid solution from amorphous to crystalline state and the coarsening of zirconia and alumina particles in the heat treatment process.

The α-Al_2O_3 powder lost 2% of its weight when was heated to 1000°C and the $ZrO_2(CeO_2, Y_2O_3)$ powder lost about 9%. In the 90AZK–58.5AZK mixtures, the weight loss increased from 2 to 4% with greater content of the zirconia-based solid solution.

Table 2 shows the phase composition of the 90AZK–58.5AZK powders after heat treatment. The alumina phase composition has no effect on the $ZrO_2(Y_2O_3, CeO_2)$ transformation when the combined method is used. Mechanical mixing, belonging to the methods to activate the starting powders, induced the metastable F-ZrO_2 $\rightarrow$ T-ZrO_2 phase transformation in the experimental conditions. Traces of M-ZrO_2 were identified in the 90AZK and 80AZK mixtures. The 90AZK and 80AZK powders did not change their phase composition in subsequent heat treatment. The M-ZrO_2 phase was not found to form in the 70AZK mixture and was identified only after heat

TABLE 2. XRD Results for the Powders Produced by HTSM and Heat Treated in the Range 400–1450°C

Temperature, °C	Powder phase composition			
	90AZK	80AZK	70AZK	58.5AZK
Starting powders	T-ZrO_2, M-ZrO_2 (tr.),* α-Al_2O_3	T-ZrO_2, M-ZrO_2 (tr.), α-Al_2O_3	T-ZrO_2, α-Al_2O_3	T-ZrO_2, α-Al_2O_3
400	T-ZrO_2, M-ZrO_2 (tr.), α-Al_2O_3	T-ZrO_2, M-ZrO_2 (tr.), α-Al_2O_3	T-ZrO_2, α-Al_2O_3	T-ZrO_2, α-Al_2O_3
550	T-ZrO_2, M-ZrO_2 (tr.), α-Al_2O_3	T-ZrO_2, M-ZrO_2 (tr.), α-Al_2O_3	T-ZrO_2, α-Al_2O_3	T-ZrO_2, α-Al_2O_3
700	T-ZrO_2, M-ZrO_2 (tr.), α-Al_2O_3	T-ZrO_2, M-ZrO_2 (tr.), α-Al_2O_3	T-ZrO_2, α-Al_2O_3	T-ZrO_2, α-Al_2O_3
850	T-ZrO_2, M-ZrO_2 (tr.), α-Al_2O_3	T-ZrO_2, M-ZrO_2 (tr.), α-Al_2O_3	T-ZrO_2, α-Al_2O_3	T-ZrO_2, α-Al_2O_3
1000	T-ZrO_2, M-ZrO_2 (tr.), α-Al_2O_3	T-ZrO_2, M-ZrO_2 (tr.), α-Al_2O_3	T-ZrO_2, α-Al_2O_3	T-ZrO_2, M-ZrO_2 (tr.), α-Al_2O_3
1150	T-ZrO_2, M-ZrO_2 (tr.), α-Al_2O_3	T-ZrO_2, M-ZrO_2 (tr.), α-Al_2O_3	T-ZrO_2,α-Al_2O_3	T-ZrO_2, M-ZrO_2 (tr.), α-Al_2O_3
1300	T-ZrO_2, M-ZrO_2 (tr.), α-Al_2O_3	T-ZrO_2, M-ZrO_2 (tr.), α-Al_2O_3	T-ZrO_2, α-Al_2O_3	T-ZrO_2, M-ZrO_2 (tr.), α-Al_2O_3
1450	T-ZrO_2, M-ZrO_2 (tr.), α-Al_2O_3	T-ZrO_2, M-ZrO_2 (tr.), α-Al_2O_3	T-ZrO_2, α-Al_2O_3	T-ZrO_2, M-ZrO_2 (tr.), α-Al_2O_3

*Phase traces.

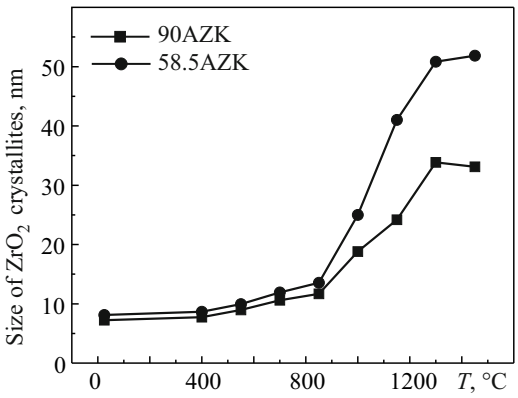

Fig. 5. Sizes of the $ZrO_2(CeO_2,Y_2O_3)$ primary particles versus heat treatment temperature

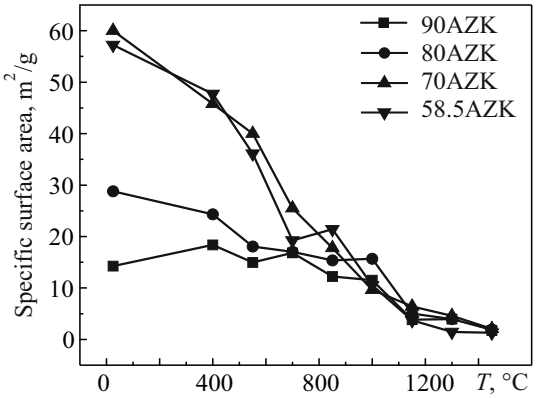

Fig. 6. Specific surface area of the ultrafine 90AZK–58.5AZK powders versus heat treatment temperature

treatment at 1000°C in the 58.5AZK mixture. These features are associated with metastable zirconia transitions under applied stresses and with particle growth at increasing temperature.

The size of primary zirconia particles in the 90AZK and 58.5AZK powders was calculated with the Scherrer equation. Conditional areas that correspond to different rates of structural changes—increase in the size of primary particles—can be determined on the temperature dependence for the sizes of $ZrO_2(CeO_2, Y_2O_3)$ primary

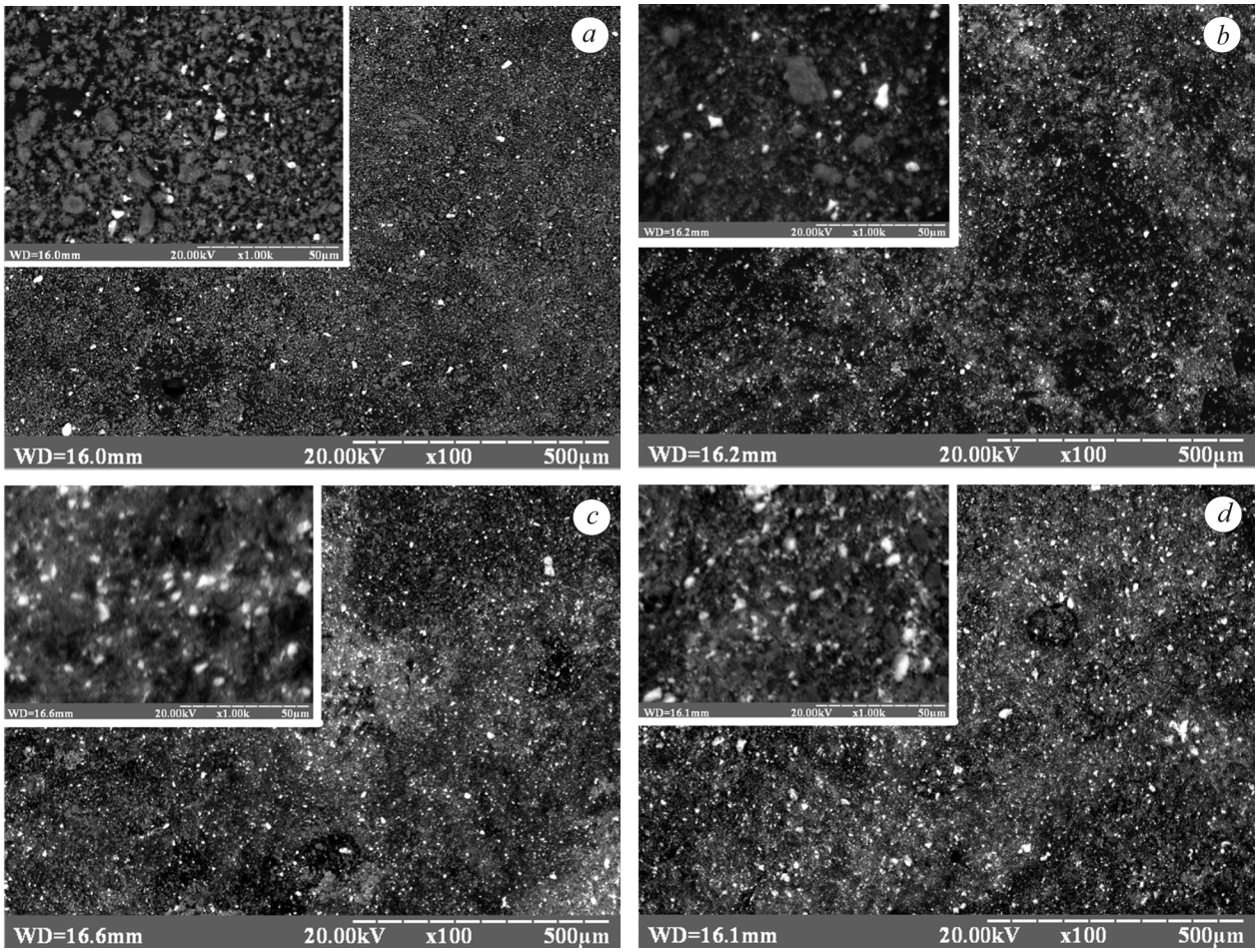

Fig. 7. SEM images of the ultrafine 90AZK (*a*), 80AZK (*b*), 70AZK (*c*), and 58.5AZK (*d*) powders after heat treatment at 400°C

particles. The sizes of $ZrO_2(CeO_2, Y_2O_3)$ primary particles hardly change in heat treatment up to 850°C and in the range 1300–1450°C (Fig. 5). The $ZrO_2(CeO_2,Y_2O_3)$ primary particles grow at the highest rate in the range 850–1300°C.

Therefore, XRD resulted in quite a contradictory finding: when $ZrO_2(CeO_2, Y_2O_3)$ content was 10 and 20 wt.%, mechanical mixing was accompanied not only by the F-ZrO_2 → T-ZrO_2 phase transformation but also partial T-ZrO_2 → M-ZrO_2 phase transformation. When the amount of $ZrO_2(CeO_2, Y_2O_3)$ increased to 30 wt.% and 41.5 wt.%, the T-ZrO_2 → M-ZrO_2 phase transformation was absent. The M-ZrO_2 phase emerged in the 58.5AZK powder only after heat treatment at 1000°C.

Figure 6 shows the specific surface area of the powders versus heat treatment temperature. According to XRD (Table 2), heat treatment induced T-ZrO_2 and traces of M-ZrO_2 in the ultrafine 90AZK and 80AZK powders, just T-ZrO_2 in the 70AZK powder, and traces of M-ZrO_2 in the 58.5AZK powder only after 1000°C. Analysis of the results (Fig. 6) indicates that dependences of the specific surface areas of the powders on heat treatment temperature correspond to the T-ZrO_2 → M-ZrO_2 phase transformation and sintering processes that occur in loose 90AZK–58.5AZK ZTA powders with increase in temperature. The specific surface area of the 90AZK and 80AZK powders is much smaller than that of the 70AZK and 58.5AZK powders up to 700°C. The bend in the range 850–1150°C (Fig. 6) is due to coarsening of the primary particles (Fig. 5) and incipient sintering of the loose powders. According to the dependences, this process intensifies after heat treatment at 1150°C. The results demonstrate that the ultrafine 90AZK, 80AZK, 70AZK, and 58.5AZK powders are highly active in sintering.

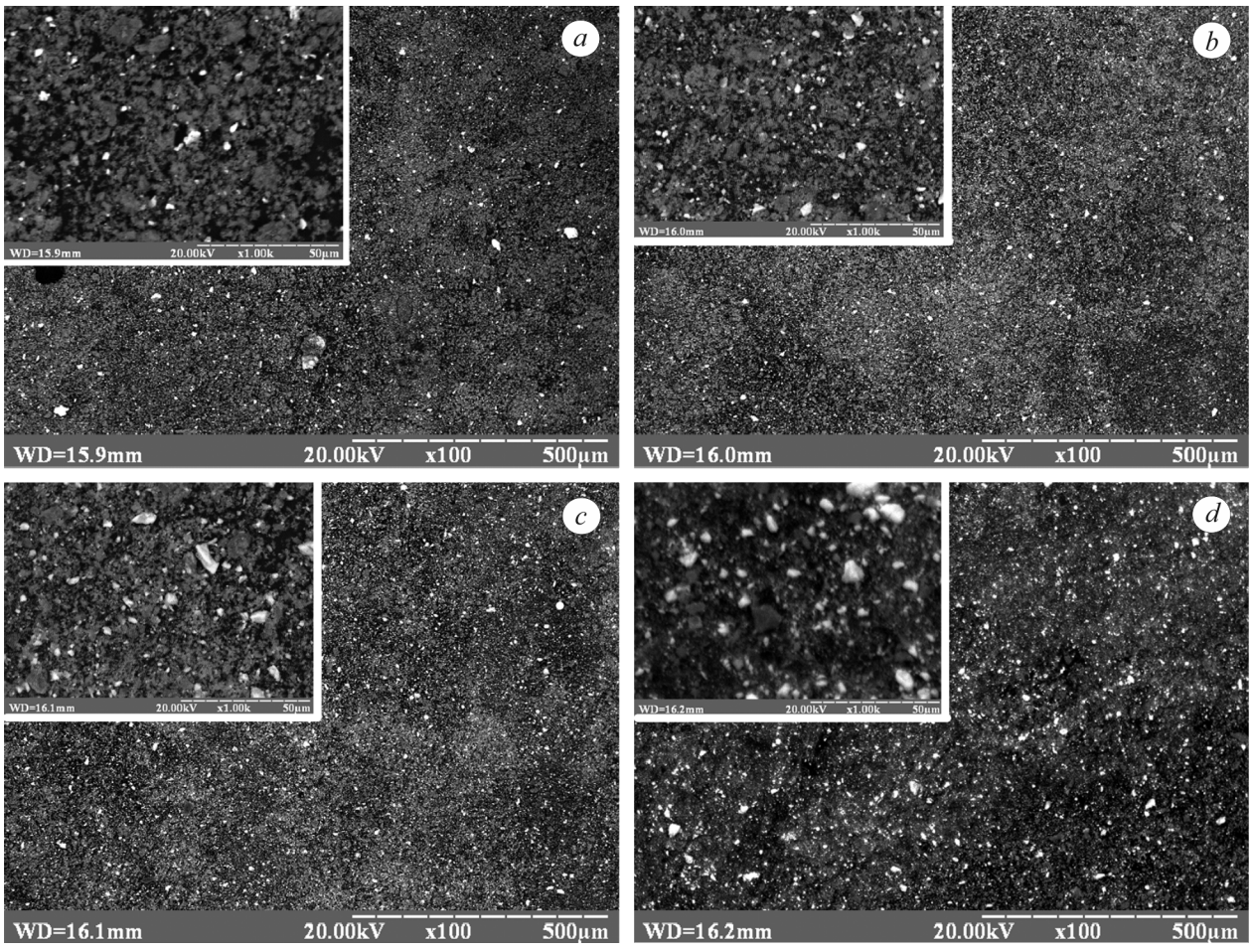

Fig. 8. SEM images of the ultrafine 90AZK (*a*), 80AZK (*b*), 70AZK (*c*), and 58.5AZK (*d*) powders after heat treatment at 850°C

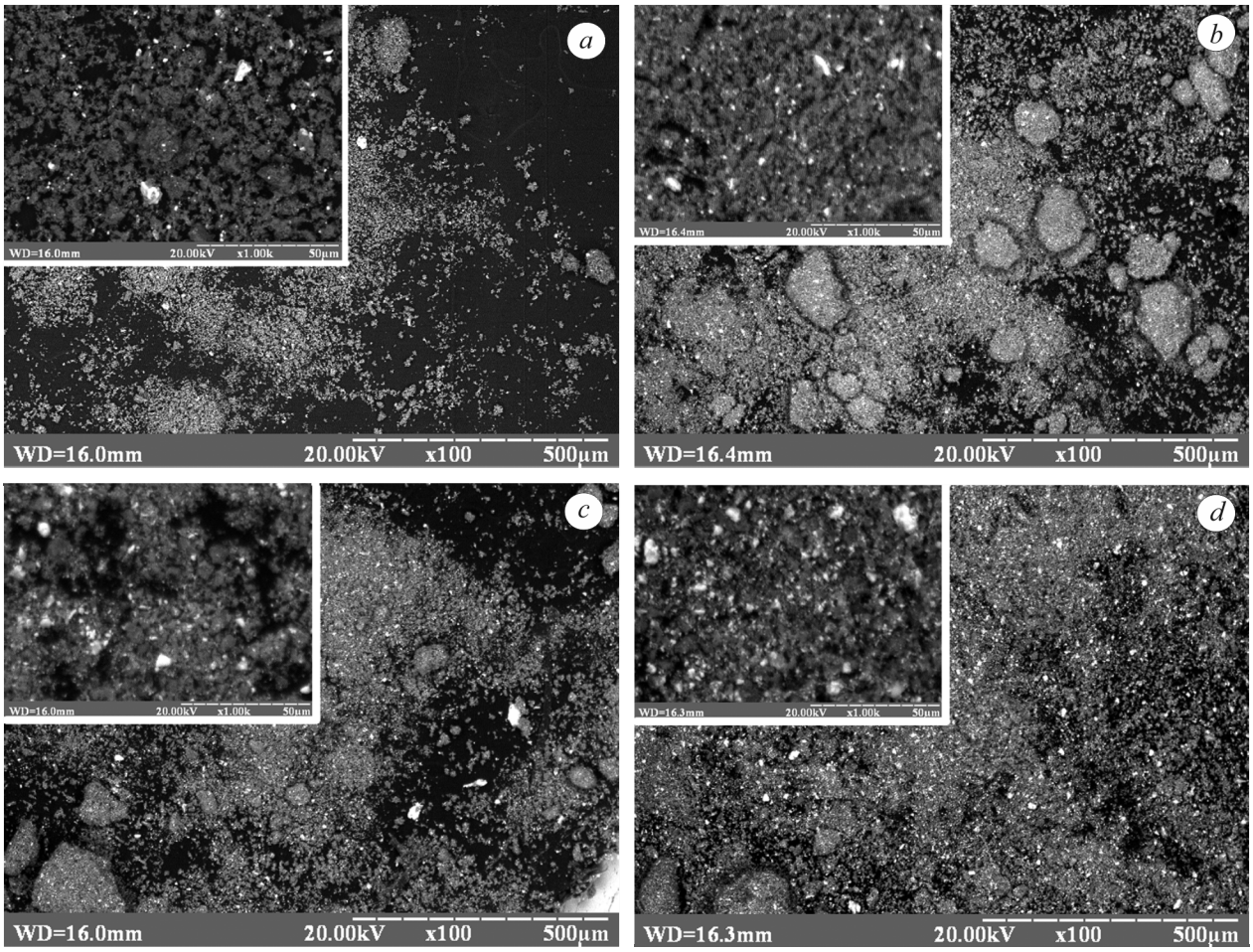

Fig. 9. SEM images of the ultrafine 90AZK (*a*), 80AZK (*b*), 70AZK (*c*), and 58.5AZK (*d*) powders after heat treatment at 1450°C

Figures 7–9 are SEM images of the ultrafine 90AZK, 80AZK, 70AZK, and 58.5AZK powders following heat treatment at 400, 850, and 1450°C. The behavior of structural components in heat treatment is primarily determined by the T-ZrO_2 → M-ZrO_2 phase transformation and sintering of loose powders.

Analysis of the data presented in Figs. 7–9 suggests that the 90AZK–58.5AZK powders change their morphology topologically continuously. The irregular agglomerates formed in mechanical mixing (Figs. 2 and 3) are retained over the entire heat treatment process but their average size reduces to 5–10 µm. Sintering of the loose powders is accompanied by decrease in the sizes of agglomerates and the formation of bonds between the agglomerates. When heat treatment temperature increases to 1300–1450°C (Fig. 9), dense agglomerates that combine the sintered conglomerates into chain-like formations show up. Note that all changes in morphology of the 90AZK–58.5AZK powders influence the dependences of the specific surface area of the powders on heat treatment temperature (Fig. 6).

Changes in the shape factor of the ultrafine 90AZK–58.5AZK powders in the heat treatment process are illustrated in Fig. 10. Dependences identical to the starting ones were obtained for each powder. Insignificant variations in the dependences (compared to those for the starting powders) result from sintering of the powders. The content of first-order agglomerates with a shape factor to 0.5 does not exceed 4%, indicating that regular agglomerates are formed. Round and polyhedral regular agglomerates mainly developed in the ultrafine 90AZK–58.5AZK powders.

The topochemical memory effect is involved in the development of ZTA materials [14]: although complex physicochemical options and mechanical and thermal impacts are used, the properties of the materials are primarily

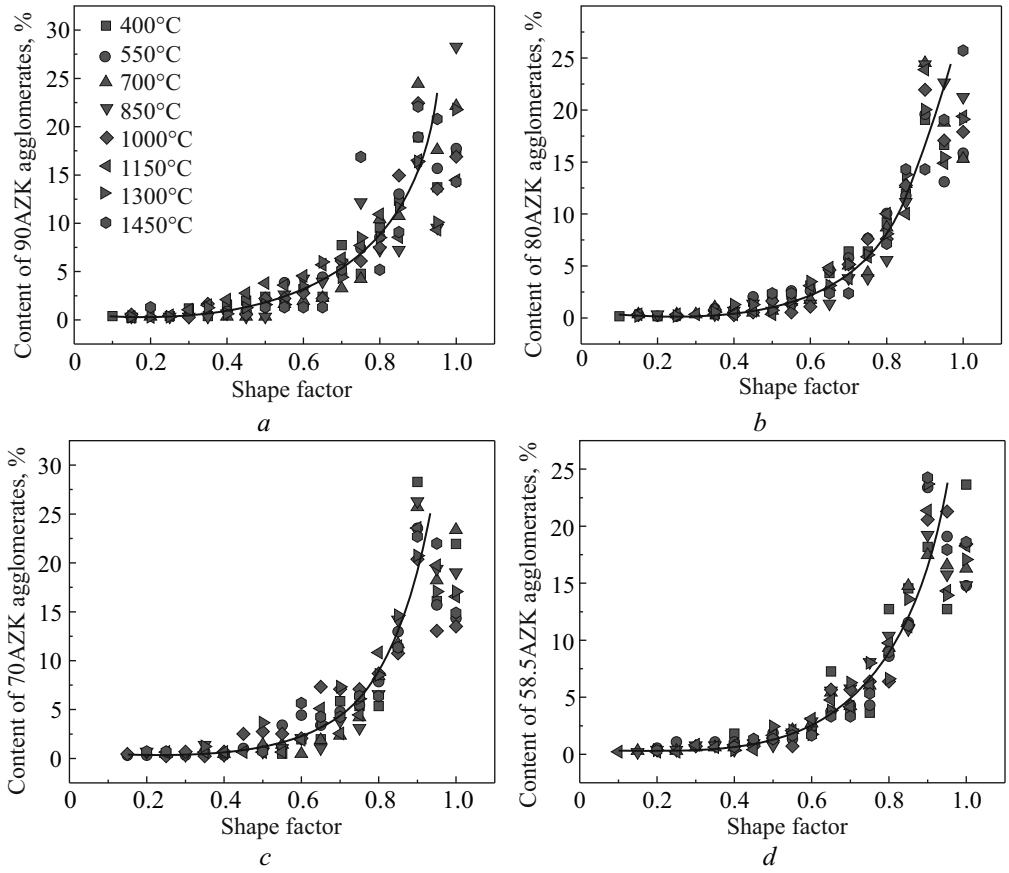

Fig. 10. Shape factor of the ultrafine 90AZK (*a*), 80AZK (*b*), 70AZK (*c*), and 58.5AZK (*d*) powders versus heat treatment temperature

determined by the properties of the starting powders (size and size distribution, specific surface area, and shape of the particles and phase composition). Analysis of the data indicates that the topochemical memory effect shows up already when the ultrafine 90AZK, 80AZK, 70AZK, and 58.5AZK powders are heat treated. This indicates that the shape factor of the ultrafine powders changes in the heat treatment in the same way as the shape factor of the starting mixtures produced by hydrothermal synthesis combined with mechanical mixing.

CONCLUSIONS

Hydrothermal synthesis combined with mechanical mixing has been employed to produce nanosized alumina powders with a high zirconia content for the development of ZTA composites with a rigid alumina matrix toughened with fine particles of the zirconia-based solid solution codoped with ceria and yttria. The physicochemical properties of the powders in the heat treatment process at 400–1450°C, which is accompanied by zirconia phase transformations and sintering, have been determined.

The F-ZrO_2 → T-ZrO_2 phase transformation proceeds fully in the mechanical mixing process. The T-ZrO_2 → M-ZrO_2 phase transformation is partial in the powders with 10 and 20 wt.% ZrO_2. When ZrO_2 content increases, the M-ZrO_2 phase forms only after 1150°C. The dependences showing the sizes of primary particles and specific surface area of the powders versus heat treatment temperature and the sharp decrease in the specific surface area in heat treatment in the range 1150–1450°C are indicative of high activity of the resultant powders in sintering.

The shape factor of the powders changes in the heat treatment process in the same way as the shape factor of the starting powders. ‘Soft’ agglomerates with a shape factor of 0.9 form in the powders, corresponding to polygonal regular agglomerates. The agglomerate distribution according to the shape factor depends on the

physicochemical processes that occur in the powders when they are heat treated. This confirms that the morphological features of the powders are determined by the method used to produce them, the phase composition of the samples being equal. The topochemical memory effect has been found in the powder heat treatment process.

These research efforts serve as a basis for microstructural design of ZTA composites for various applications that possess the required mechanical properties.

REFERENCES

1. R.H.J. Hannink, P.M. Kelly, and B.C. Muddle, "Transformation toughening in zirconia-containing ceramics," *J. Am. Ceram. Soc.*, **83**, No. 3, 461–487 (2000).
2. J. Chevalier and L. Gremillard, "Zirconia as a biomaterial," *Ref. Mod. Mater. Sci. Mater. Eng. Compr. Biomater. II*, **1**, 122–144 (2017): https://doi.org/10.1016/B978-0-12-803581-8.10245-0.
3. J. Chen, Z. Xie, W. Zeng, and W. Wu, "Toughening mechanisms of ZTA ceramics at cryogenic temperature (77 K)," *J. Ceram. Int.*, **43**, Issue 5, 3970–3974 (2017): http://dx.doi.org/10.1016/j.ceramint.2016.11.072.
4. Ernesto Byron Benalcazar Jalkh, Kelli Nunes Monteiro, Paulo Francisco Cesar, Luis Antonio Genova, Edmara T.P. Bergamo, Adolfo Coelho de Oliveira Lopes, Erick Lima, Paulo Noronha Lisboa-Filho, Tiago Moreira Bastos Campos, Lukasz Witek, Paulo G. Coelho, Ana Flavia Sanches Borges, and Estevam A. Bonfante, "Aging resistant ZTA composite for dental applications: Microstructural, optical and mechanical characterization," *J. Dental Mater.*, **36**, Issue 9, 1190–1200 (2020): https://doi.org/10.1016/j.dental.2020.05.011.
5. J. Chevalier and L. Gremillard, "Ceramics for medical applications: A picture for the next 20 years," *J. Eur. Ceram. Soc.*, **29**, Issue 7, 1245–1255 (2009).
6. N.V. Sharova, N.A. Popova, and E.S. Lukin, "Effect of a eutectic addition in the Al_2O_3–ZrO_2–Y_2O_3 system on the properties of corundum ceramics," *Usp. Khim. Khim. Tekhnol.*, **31**, No. 3, 119–121 (2017).
7. V.V. Kulyk, Z.A. Duriagina, B.D. Vasyliv, V.I. Vavrukh, P.Ya. Lyutyy, T.M. Kovbasiuk, and M.Ya. Holovchuk, "Effects of yttria content and sintering temperature on the microstructure and tendency to brittle fracture of yttria-stabilized zirconia," *Arch. Mater. Sci. Eng.*, **109**, No. 2, 65–79 (2021): https://doi.org/10.5604/01.3001.0015.2625.
8. A.K. Pandey, U.R. Jena, and K. Biswas, "In vitro ageing and wear behavior of ceria stabilized zirconia toughened alumina (CSZ-TA) bio-ceramic," *Mater. Chem. Phys.*, **146**, 456 (2014).
9. N.A. Rejab, A.Z.A. Azhar, K.S. Kian, M.M. Ratnam, and Z.A. Ahmad, "Effects of MgO addition on the phase, mechanical properties, and microstructure of zirconia-toughened alumina added with CeO_2 (ZTA-CeO_2) ceramic composite," *Mater. Sci. Eng. A*, **595**, 18–24 (2014).
10. N.A. Rejab, A.Z.A. Azhar, M.M. Ratnam, and Z.A. Ahmad, "The effects of CeO_2 addition on the physical, microstructural and mechanical properties of yttria stabilized zirconia toughened alumina (ZTA)," *Int. J. Refract. Met. Hard Mater.*, **36**, 162–166 (2013).
11. V. Ponnilavan and S. Kannan, "Structural, morphological and mechanical characteristics on the role of excess ceria additions in zirconia toughened alumina systems," *J. Alloys Compd.*, **694**, 1073–1082 (2017).
12. A.M. Abyzov, "Latest research on the development of high-quality aluminum-oxide ceramics (Review). Part 2. Synthesis and sintering of nanopowders, sol-gel and other methods of producing finely disperse and fibrous aluminum oxide," *Glass Ceram.*, **75**, No. 9–10, 352–362 (2019).
13. M.Y. Smyrnova-Zamkova, O.K. Ruban, O.I. Bykov, and O.V. Dudnik, "Physicochemical properties of fine-grained powder in Al_2O_3–ZrO_2–Y_2O_3–CeO_2 system produced by combined method," *Compos. Theory Pract.*, **18**, No. 4, 234–240 (2018).
14. Yu.D. Tretiakov, "New generations of ceramics," *Vest. AN SSSR*, No. 2, 98–111 (1987).
15. M.M. Basha, S.M. Basha, B.K. Singh, N. Mandal, and M.R. Sankar, "A review on synthesis of zirconia toughened alumina (ZTA) for cutting tool applications," *Mater. Today: Proc.*, **26**, Part 2, 534–541 (2020).

16. E.V. Dudnik, S.N. Lakiza, Ya.S. Tishchenko, A.K. Ruban, V.P. Redko, A.V. Shevchenko, and L.M. Lopato, “Phase diagrams of refractory oxide systems and microstructural design of materials,” *Powder Metall. Met. Ceram.*, **53**, No. 5–6, 303–311 (2014).
17. K.C. Patil, S.T. Aruna, and S. Ekamtaran, “Combustion synthesis,” *Curr. Opin. Solid State Mater. Sci.*, No. 2, 158–165 (1997).
18. M.Yu. Smirnova-Zamkova, *Effect of Production Methods on the Physicochemical Properties of Nanocrystalline Powders in the Al_2O_3–ZrO_2–Y_2O_3–CeO_2 System: Author’s Abstract of PhD Thesis in Chemistry* [in Ukrainian], Inst. Probl. Materialoznav. NAN Ukrainy, Kyiv (2021), p. 25.
19. Yu.D. Tretiakov and V.I. Putliaev, *Introduction to the Chemistry of Solid-State Materials: University Book* [in Russian], Nauka, Moscow (2006), p. 400.
20. E.V. Dudnik, S.N. Lakiza, V.V. Tsukrenko, Ya.S. Tishchenko, A.K. Ruban, and V.P. Redko, “Nanocrystalline oxide powders for microstructural design of materials,” *Nanosyst. Nanomater. Nanotekhnol.*, **14**, No. 4, 561–575 (2016).
21. F. Trubelja and V. Stubican, “Phase equilibria and ordering in the system zirconia-hafnia-yttria,” *J. Am. Ceram. Soc.*, **71**, No. 8, 662–666 (1988).
22. I.O. Marek, O.K. Ruban, V.P. Redko, M.I. Danilenko, S.A. Korniy, and O.V. Dudnik, “Physicochemical properties of hydrothermal nanocrystalline ZrO_2–Y_2O_3–CeO_2 powders,” *Powder Metall. Met. Ceram.*, **58**, No. 3–4, 125–132 (2019).
23. O.I. Khomenko and O.V. Khomenko, “Use of the AMIC software for quantitative metallography,” in: *Mathematical Models and Computational Experiment in Materials Science*, Proc. Inst. Materialoznav. NAN Ukrainy, Issue 16, 35–42 (2014).
24. V.V. Panichkina and I.V. Uvarova, *Methods for Controlling the Particle Size and Specific Surface Area of Metallic Powders* [in Russian), Nauk. Dumka, Kyiv (1973), p. 168.